Electronic Supplementary Material

Precisely Design of Fe_x (x=1~2) Cluster Nanocatalysts for Effective Tumor Nanocatalytic Therapy

Yanfei Meng[1†], Dongsheng Zhang[1†], Yingzi Song[1], Xinyi Yang[1], Yongli Gao[4], Jun Ma[2*], Zunfu Hu[1,3*] and Xiuwen Zheng[1,2*]

1. Key Laboratory of Functional Nanomaterials and Technology in Universities of Shandong, Linyi University, Linyi 276000, P.R. China

2. Medical College of Linyi University, Linyi 276000, P.R. China

3. School of Materials Science and Engineering, Linyi University, Linyi 276000, P. R. China

4. Linyi People's Hospital, Linyi 276000, P. R. China

Table of Contents

1. Synthesis and Characterization

1. 1 Main reagents

Zinc nitrate hexahydrate $Zn(NO_3)_2•6H_2O$, AR, Sinopharm), diiron nonacarbonyl ($Fe_2(CO)_9$, ≥97.0%, Macklin), 2-methylimidazole (98%, Aldrich), methanol (AR, Sinopharm), sodium hydroxide (NaOH, AR, Sinopharm), hexadecyl trimethyl ammonium bromide (CTAB, ≥ 99%, Aldrich), tetraethyl orthosilicate (TEOS, AR, Aldrich), tamoxifen (TAM, ≥99%, Aldrich), DSPE-PEG-FA (M_v=2000, Sigma), DSPE-PEG-DSPE (M_v=2000, Sigma).

1.2 Synthesis of Fe_1-N-C

$Zn(NO_3)_2•6H_2O$ (9519.68 mg) and $Fe(acac)_3$ (128 mg) were dissolved in methanol solution (500 mL), and 2-methylimidazole (11083.5 mg) was dispersed in methanol solution (400 mL). Subsequent these solutions were mixed uniformly and stirred rapidly at room temperature. After 2 h stirring, the mixture was then the aging reaction for 6 h. The $Fe(acac)_3$-ZIF-8 was collected by centrifugation and washed with methanol until the supernatant was colorless.

The $Fe(acac)_3$-ZIF-8 was dispersed in 240 mL of 10 vol% methanol and the pH of the mixture was adjusted to 11 with NaOH aqueous (1 mol L^{-1}). Then CTAB (0.408 mM) and TEOS (1.2 mL) were added, followed by stirring rapidly for 30 minutes. The $Fe(acac)_3$-ZIF-8@$mSiO_2$ was collected by centrifugation and washed three times with methanol, then dried at 60°C.

The dried $Fe(acac)_3$-ZIF-8@$mSiO_2$ powder was pyrolyzed at 800 °C under argon atmosphere for 180 min with a heating rate of 2 °C min^{-1}, and then cooled to room temperature naturally. The obtained Fe_1-N-C@$mSiO_2$ was etched with NaOH aqueous (1 mol L^{-1}) for 3 h then washed with water and ethanol until until the supernatant to neutral.

1.3 Preparation of Fe_1@DF NEs

Fe_1-N-C (10 mg), DSPE-PEG-DSPE (40 mg), and DSPE-PEG-FA (20 mg) were completely dissolved in water, respectively, and then mixed evenly and continuously ultrasonic for 30 min and stirred 2 h away from light. Finally, Fe_1@DF NEs were obtained after centrifugal washing.

1.4 Preparation of Fe_2@DF NEs

Fe_2-N-C (10 mg), DSPE-PEG-DSPE (40 mg), and DSPE-PEG-FA (20 mg) were completely dissolved in water, respectively, and then mixed evenly and continuously ultrasonic for 30 min and stirred 2 h away from light. Finally, Fe_2@DF NEs were obtained after centrifugal washing.

1.5 Characterizations

The TEM and Mapping elemental characterization of the material were carried out on a TEM (JEOL JEM-2100) with a field emission gun operating at 200 kV; spherical aberration-corrected high-angle annular dark-field scanning TEM (HAADF-STEM) images are in The spherical aberration-corrected transmission electron microscope (JEM-ARM200F) of 200 kV was obtained; the UV-vis absorption spectrum was obtained on the UV-visible spectrophotometer (NANO DROP 2000); the Zeta potential of the material was measured by a nanoparticle size and potential analyzer (Nano-ZS); crystal structure was characterized on X-ray powder diffraction (D8 Advae, Bruker,

Switzerland); X-ray photoelectron spectroscopy (XPS) was tested on electron spectroscopy (Oxford); electron spin resonance Spectroscopy (ESR) was measured using Bruker EMXPLUS; elemental content was measured by inductively coupled plasma mass spectrometry (ICP-MS, iCAP Q, Thermo Flsher); thermal images were recorded using a FLIR T420 thermal imager.

2. Experimental Peocedures

2.1 •OH detection

DMPO was used as •OH trapping agent, pH=5.8 PBS as buffer solution. Add 50 μL H_2O_2 solution (200 mM) and 100 μL Fe_1-N-C (109 μg mL^{-1}, 0.375%) or Fe_2-N-C (100 μg mL^{-1}, 0.41%) to 1 mL tube, then add 100 μL DMPO solution. After 5-10 s of vortex oscillation, the liquid was transferred to a glass capillary for ESR detection. For blank samples, Fe based materials were not added.

2.2 Peroxidase-like activity and kinetic assay.

Fe_x-N-C (100 μg mL^{-1}), H_2O_2 (10 mM), and TMB (50 μg mL^{-1}) were added to 2 mL of PBS solution (pH 5.8). The absorbance of the color reactions was recorded after a certain reaction time using a UV-vis spectrophotometer.

Additionally, the steady-state kinetic analysis was performed at 25°C in PBS solution (pH 5.8) with Fex-N-C (100 μg mL^{-1}) as a catalyst in the existence of TMB (100 μg mL^{-1}) and different concentrations of H_2O_2 (1.0, 2.5, 5.0, 10, 25 and 50 mM). The rates were plotted against H_2O_2 content and then fitted with the Michaelis-Menten curves (**Fig. S16b**). Furthermore, a linear double-reciprocal plot was used for determining the Km and V_{max} (**Fig. S16c**).

$$A = \varepsilon bc$$

$$v_0 = \frac{v_{max} \cdot [S]}{K_m + [S]}$$

$$\frac{1}{v_0} = \frac{K_m}{v_{max}} \cdot \frac{1}{[S]} + \frac{1}{v_{max}}$$

Where ν represents the initial velocity, K_m represents the Michaelis constant, [S] is the concentration of substrate, and V_{max} is the maximal reaction velocity.

2.3 Density functional theory computational method

We have employed the first-principles [1,2] to perform spin-polarization density functional theory (DFT) calculations within the generalized gradient approximation (GGA) using the Perdew-Burke-Ernzerhof (PBE) [3] formulation. We have chosen the projected augmented wave (PAW) potentials [4,5] to describe the ionic cores and take valence electrons into account using a plane wave basis set with a kinetic energy cutoff of 450 eV. Partial occupancies of the Kohn-Sham orbitals were allowed using the Gaussian smearing method and a width of 0.05 eV. The electronic energy was considered self-consistent when the energy change was smaller than 10^{-5} eV. A geometry optimization was considered convergent when the energy change was smaller than 0.05 eV $Å^{-1}$. In our structure, the U correction is used for Fe atoms. The vacuum spacing in a direction perpendicular to the plane of the structure is 20 Å for the surfaces. The Brillouin zone integration is performed using 3×3×1

Monkhorst-Pack k-point sampling for a structure. Finally, the adsorption energies(Eads) were calculated as $E_{ads}= E_{ad/sub} -E_{ad} -E_{sub}$, where $E_{ad/sub}$, E_{ad}, and E_{sub} are the total energies of the optimized adsorbate/substrate system, the adsorbate in the structure, and the clean substrate, respectively. The free energy was calculated using the equation:

$$G = E_{ads} + ZPE - TS$$

where G, E_{ads}, ZPE and TS are the free energy, total energy from DFT calculations, zero-point energy and entropic contributions, respectively.

2.4 Photothermal study

Fe_2-N-C solutions (400 μL) with different concentrations (0, 50, 100 and 200 μg mL^{-1}) were irradiated with an 808 nm laser (1.0 W cm^{-2}) for 5 min, and the temperature changes were monitored with an infrared thermal imager. The photothermal properties of Fe_2-N-C solution (200 μg mL^{-1}) under different laser power densities (0.3, 0.5 and 1.0 W cm^{-2}, respectively) were determined by the same method. To study the photothermal conversion effect, Fe_2-NC solution (200 μg mL^{-1}, 400 μL) was irradiated with 808 nm (1 W cm^{-2}) laser for 5 min, then the near-infrared laser was turned off, and the temperature was monitored with an infrared thermal imager.

2.5 Photothermal conversion efficiency

Fe_2-N-C solutions (500 μL) with different concentrations (0, 50, 100, and 200 μg mL^{-1}) were irradiated with 808 nm laser (1.0 W cm^{-2}) for 6 min, and the temperature changes were monitored with an infrared thermal imager. The photothermal properties of Fe_2-N-C solution (200 μg mL^{-1}) under different laser power densities (0.3, 0.5, and 1.0 W cm^{-2}, respectively) were measured by the same method. To study the photothermal conversion effect, Fe_2-N-C solution (200 μg mL^{-1}, 500 μL) was irradiated with 808 nm (1 W cm^{-2}) laser for 5 min, then the near-infrared laser was turned off, and the temperature change was monitored with an infrared thermal imager.

Calculation of photothermic conversion efficiency (η) of Fe_2-N-C:

$$\eta = \frac{hA(T_{max} - T_{sur}) - Q_s}{I(1 - 10^{-A_{808}})}$$

T_{max} represents the maximum equilibrium temperature; T_{sur} is the ambient temperature. Q_s represent the heat loss due to light absorption by the container. I is the incident laser power. A_{808} is the absorbance of the sample at 808 nm. h is the heat transfer coefficient, A is the surface area of the container, and hA is calculated from **Figure S29** according to equation:

$$hA = \frac{m_s C_s}{\tau_s}$$

τ_s represents the sample system time constant, m_s and C_s are the mass and heat capacity of the solvent. According to the calculation, the η of the sample is calculated to be 46.8%.

2.6 loading efficiency of TAM

The loading efficiency of TAM was determined by UV-vis spectrophotometry. The tamoxifen was

dissolved in a methanol solution, and the volume was fixed to 10 mL to obtain 0.5g L^{-1} tamoxifen solution. After that, 0.1, 0.2, 0.3, 0.4, 0.5, and 0.6mL of control solution were accurately absorbed and filled with methanol to 5mL in test tubes. The absorbance was determined by spectrophotometry at the maximum absorption wavelength of tamoxifen. The standard curve as follows showed the linear relationship between absorbance and TAM concentration in methanol solution, and the relationship conforms to Lambert's Law:

$$A = 0.01979 + 53.182\ c$$

where A is the absorbance value and c is the mass concentration of TAM.

According to the absorbance value of the initial solution of TAM at 238 nm and the supernatant solution after reaction at the corresponding wavelength, the loading rate of TAM on Fe_2@TDF NEs was calculated to be about 60.9 % according to the following equation:

$$TAM\ loading\ rate\ (\%) = \frac{initial\ mass\ of\ TAM - mass\ of\ TAM\ in\ supernatant\ after\ reaction}{initial\ mass\ of\ TAM} \times 100\%$$

2.7 Cell culture

All cells were cultured in DMEM medium containing 2% penicillin/streptomycin and 12% fetal bovine serum at 37°C in a cell incubator in a 5% CO_2 atmosphere.

2.8 Cytotoxicity assay

Three experimental groups were set up, each with 9 replicate wells. Different materials (1) PBS; (2) Fe_2@DF (100 μg mL^{-1}); (3) Fe_2@TDF (100 μg mL^{-1}) were incubated with cells for 4 h, respectively. Then it was divided into 2 groups with 4 multiple holes in each group, and one group was irradiated with 808 laser light (0.5 W cm^{-2}, 5 min). Culture was continued for 20 h, and the cell viability was determined by WST-1 method.

2.9 The cell fluorescence images

DSPE-PEG-FITC was attached to the material to study the material uptake capacity of its cells. After 4T1 cells were cultured in 6-well plates for a certain period of time, they were incubated with Fe_2@TDF-FITC (200 μg mL^{-1}) for 0.5 h, 1 h, 2 h and 4 h, respectively. This was followed by several washes with PBS to remove excess material. Then DAPI was added to each well for 20 min. The supernatant was aspirated, washed twice with PBS, and then 1 mL PBS was added and observed under a fluorescence microscope.

After culturing 4T1 cells in a 6-well culture plate for a certain period of time, use (1) PBS; (2) Fe_2@DF (100 μg mL^{-1}); (3) Fe_2@TDF (100 μg mL^{-1}); (4) Fe_2@TDF+laser (0.5 W cm^{-2}, 5 min) treatment. Incubate with AM and PI staining solution for 30 min and observe under a fluorescence microscope.

4T1 cells were treated with (1) PBS; (2) TAM (200 μg mL^{-1}); (3) Fe_2@TDF (100 μg mL^{-1}); (4)

Fe_2@TDF+laser (0.5 W cm^{-2}, 5 min) treatment. After washing with PBS, add 1 mL cell culture medium and 1 μL BCECF-AM, and incubate in a cell incubator at 37 ºC for 40 min. After washing twice with PBS, 1 mL PBS and 1 μL DAPI were added to each well, incubated in the dark for 20 min, and observed under a fluorescence microscope.

4T1 cells were treated with (1) Fe_1@DF (109 μg mL^{-1}); (2) Fe_2@DF (100 μg mL^{-1}); (3) Fe_2@TDF (100 μg mL^{-1}); (4) Fe_2@TDF+laser (808 nm, 0.5 W cm^{-2}, 5 min) treatment. Add 1 mL cell culture medium and 1 μL DCFH-DA, incubate for 40 min and observe under a fluorescence microscope.

4T1 cells were treated with (1) Fe_2@DF (100 μg mL^{-1}); (2) Fe_2@TDF (100 μg mL^{-1}); (3) Fe_2@TDF+laser (0.5 W cm^{-2}, 5 min) treatment. Add 1 mL cell culture medium and 1 μL C11-BODIPY to incubate for 40 min and observe under a fluorescence microscope.

4T1 cells were treated with (1) PBS; (2) TAM (200 μg mL^{-1}); (3) Fe_2@TDF (100 μg mL^{-1}); (4) Fe_2@TDF+laser (0.5 W cm^{-2}, 5 min) treatment. Then, 0.5 mL cell culture medium and 0.5 mL JC-1 working solution were added to incubate for 20 min. Washed twice with 4°C JC-1 staining buffer and observed under a fluorescence microscope.

2.10 Detection of intracellular GSH

4T1 cells were cultured in a 6-well plate (1×10^5 cells per well) and treated with (1) PBS; (2) Fe_1@DF (109 μg mL^{-1}); (3) Fe_2@ DF (100 μg mL^{-1}) treatment. The content of intracellular GSH was detected using the GSH detection kit according to the instructions.

2.11 Western blot analysis

4T1 cells were cultured in 6-well plates (1×10^5 cells per well) and treated with (1) PBS; (2) 808 nm (0.5 W cm^{-2}, 5 min), Fe_2@DF (200 μg mL^{-1}) and Fe_2@DF + laser was treated separately. Cells were then harvested with trypsin and lysed in lysis buffer. The protein content was detected by BCA protein method. The proteins were then separated by sodium dodecyl sulfate-polyacrylamide gel electrophoresis (SDS-PAGE) and transferred to polyvinylidene difluoride (PVDF) membranes. After blocking with 5% dry skim milk for 1 h, the membrane was incubated with the corresponding primary antibody on a shaker at 4°C overnight, followed by secondary antibody incubation (1 h at room temperature). Then, the membranes were visualized by the ECL plus detection system.

2.12 Bio-TEM analysis

4T1 cells were placed in a petri dish (1×10^6 cells) and treated with PBS and Fe_2@TDF (100 μg mL^{-1}) for 12 h respectively. Cells were subsequently collected for biological transmission electron microscopy imaging.

2.13 Antitumor therapy strategy

Female BALB/c mice, 6 weeks old, average weight 17-22 g, from Jinan Pengyue Laboratory Animal Breeding Co., Ltd. All experiments involving animals were kept in strict accordance with the relevant regulations and requirements of the Animal Experiment Center of Linyi University.

A tumor-bearing mouse model was established by subcutaneously injecting 4T1 cells into the right hind leg of BALB/c mice. When the tumor grew to a certain volume, the tumor-bearing mice

were randomly divided into 6 groups with 5 mice in each group: (1) PBS; (2) TAM (200 μg mL^{-1}); (3) Fe_1@DF (546 μg mL^{-1}); (4) Fe_2@DF (500 μg mL^{-1}); (5) Fe_2@TDF (500 μg mL^{-1}); (6) Fe_2@TDF+laser (0.5 W cm^{-2}, 5 min). All materials were injected intravenously, with the exception of TAM, which was injected intratumorally. Treatment every 5 days for a total of 3 times.

Body weight and tumor size were recorded every two days after starting treatment, and the formula was as follows:

$$V = W^2 \times L \times 0.5$$

where V is the tumor volume, *W* is the tumor width, and *L* is the tumor length.

After 15 days, each mouse was euthanized, and its main organs (heart, liver, spleen, lung, kidney) and tumor tissues were removed, fixed with 4% paraformaldehyde at 4 °C for 24 h, and sliced for H&E. and TUNEL staining. Subsequently, nuclei were stained with DAPI. Tumor sections were photographed with a fluorescence microscope.

2.14 Hemolysis assay

Taking water as the positive control, PBS as the negative control, and different concentrations of Fe_2@TDF materials as the experimental group, they were incubated with the treated red blood cell suspension for 4 h, the samples were centrifuged and the UV-vis absorbance of the supernatants at 540 nm was measured. The hemolysis rate is calculated by the following formula:

$$Hemolysis\ Rtate\ (\%) = \frac{A_{b_{sample}} - A_{b_{negative}}}{A_{b_{positive}} - A_{b_{negative}}} \times 100\%$$

2.15 In vivo bio-distribution Study

After 7 days treatment, major organs (heart, liver, spleen, lung, and kidney) were collected and fixed in 4% neutral-buffered formalin. After weighting, 10% of the weight was solubilized in 1 mL of aqua regia under heating for 1 h and then diluted with DI water to 50 mL for the measurement Fe by ICP-MS.

3. Supplementary Figures and Tables

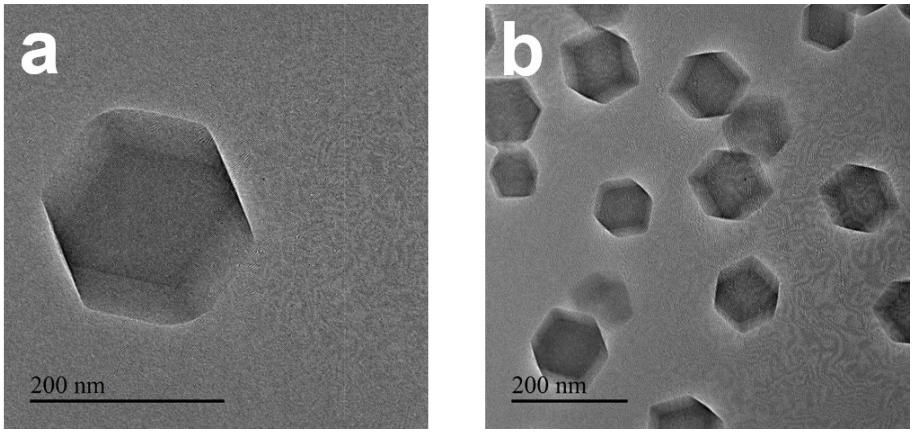

Fig. S1 TEM images of $Fe_2(CO)_9$-ZIF-8.

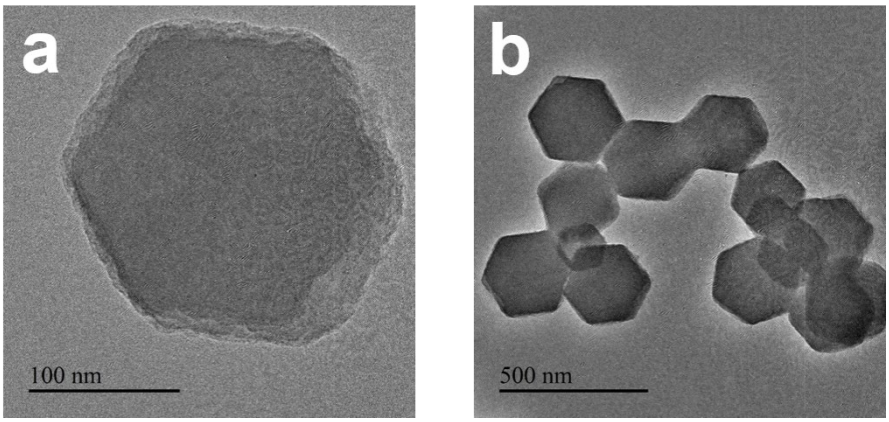

Fig. S2 TEM images of $Fe_2(CO)_9$-ZIF-8@mSiO_2.

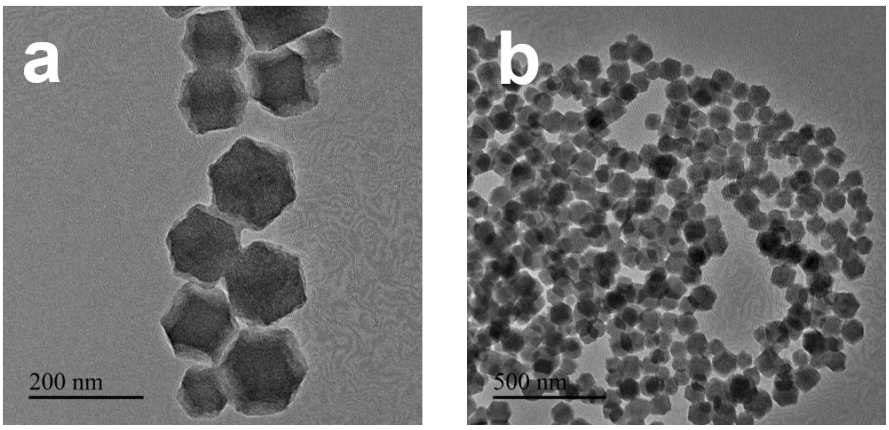

Fig. S3 TEM images of Fe_2-N-C@mSiO_2.

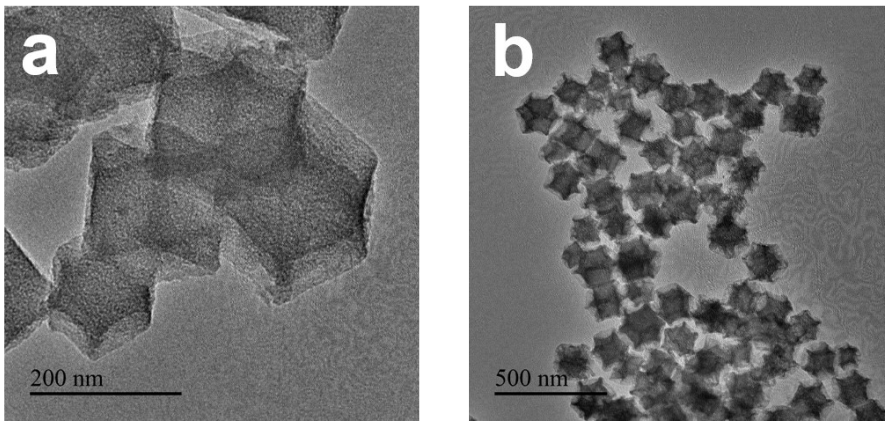

Fig. S4 TEM images of Fe_2-N-C.

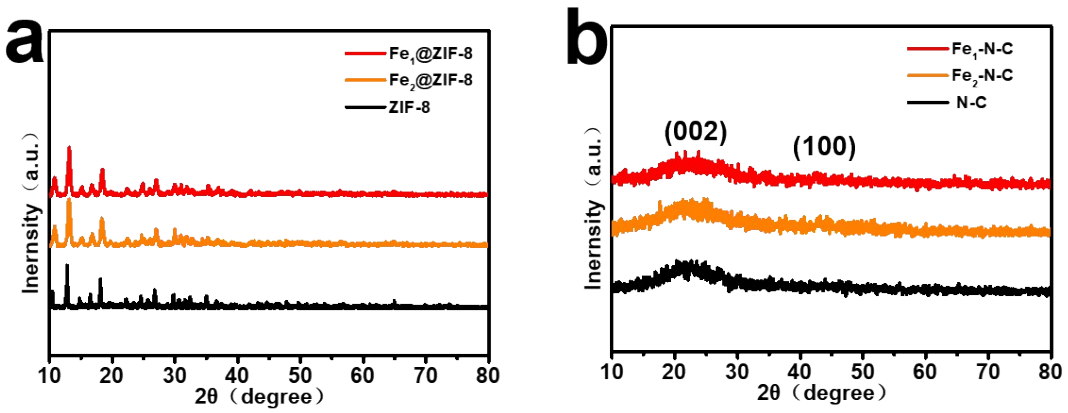

Fig. S5 (a)XRD pattern of ZIF-8, $Fe(acac)_3$-ZIF-8, and $Fe_2(CO)_9$-ZIF-8 N-C. (b) XRD pattern of N-C, Fe_1-N-C and Fe_2-N-C.

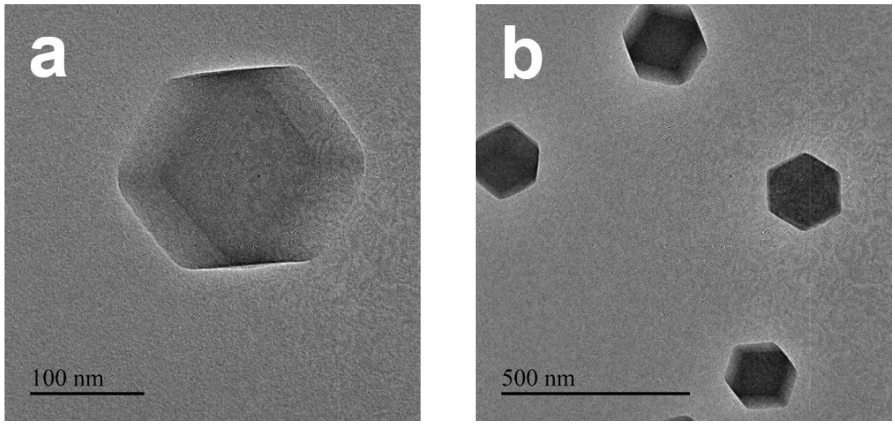

Fig. S6 TEM images of $Fe(acac)_3$-ZIF-8.

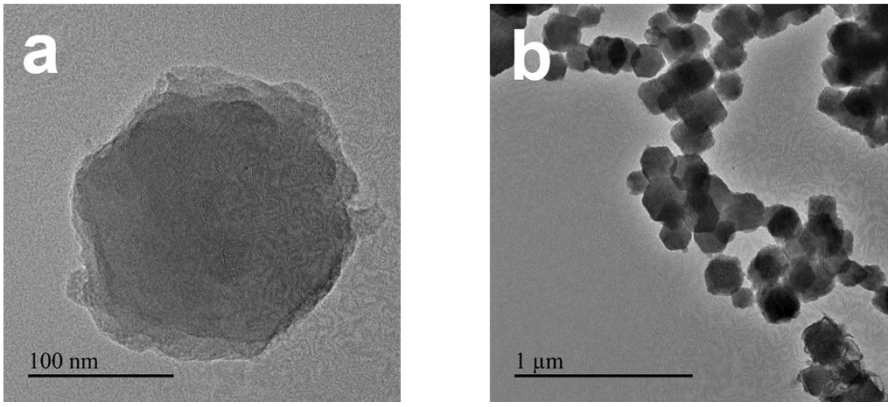

Fig. S7 TEM images of $Fe(acac)_3$-ZIF-8@$mSiO_2$.

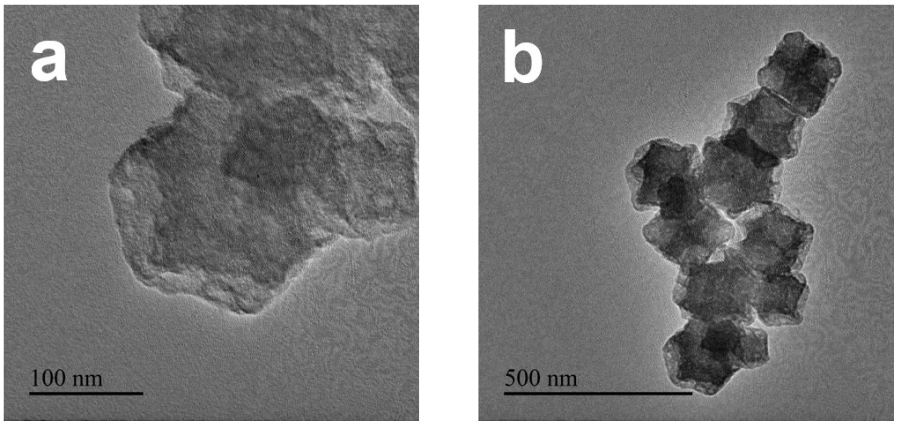

Fig. S8 TEM images of Fe_1-N-C@mSiO_2.

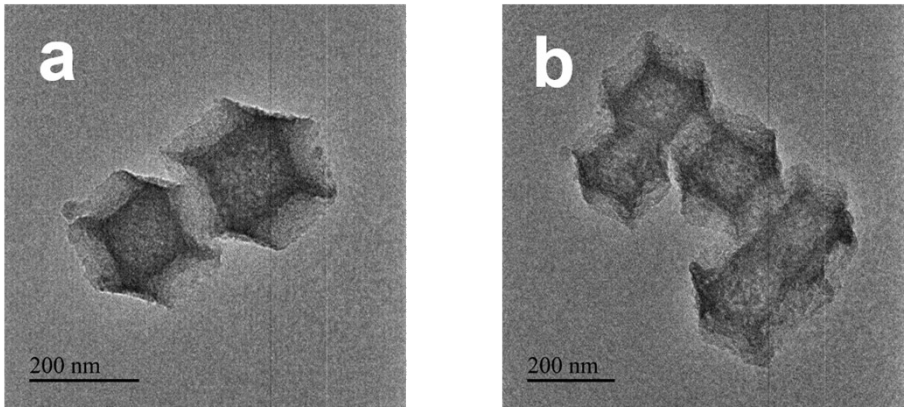

Fig. S9 TEM images of Fe_1-N-C.

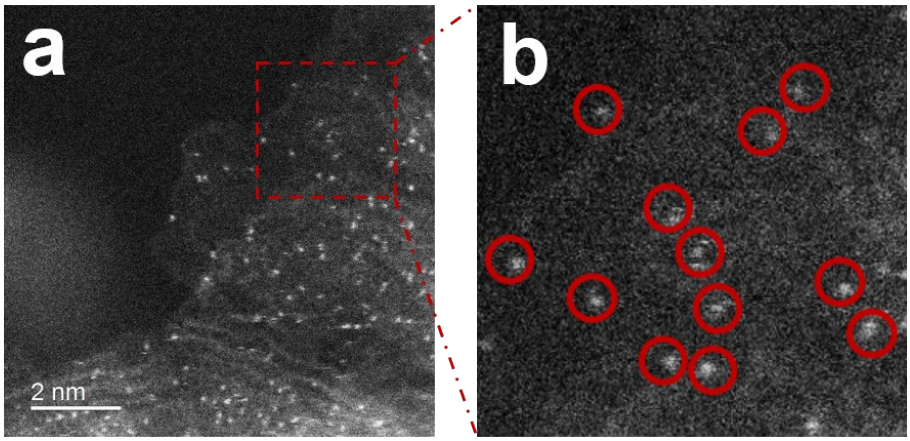

Fig. S10 (a) Atomic-resolution HADDF-STEM images of Fe_1-N-C. (g) Magnified atomic-resolution HAADF-STEM images of Fe_1-N-C.

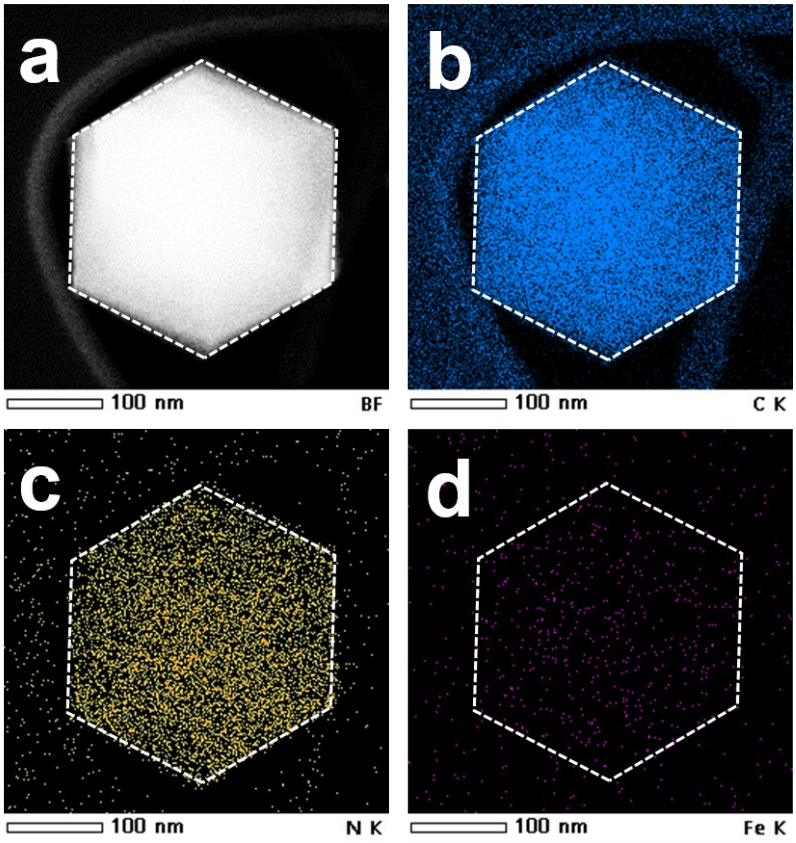

Fig. S11 (a) HAADF-STEM images of Fe_1-N-C. (b) The elemental mapping of Fe_1-N-C (including C, N and Fe elements).

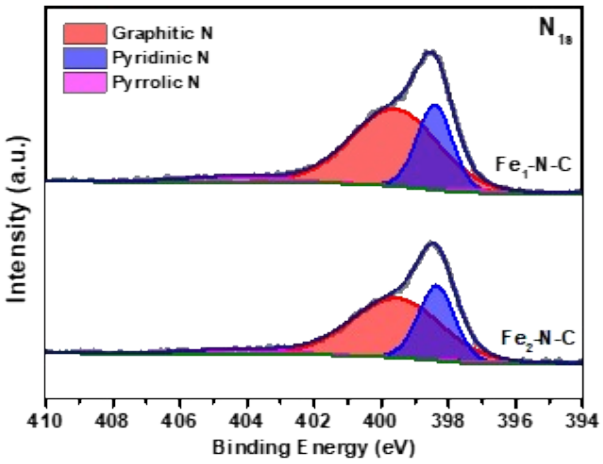

Fig. S12 XPS characterization of Fe_x-N-C sample.

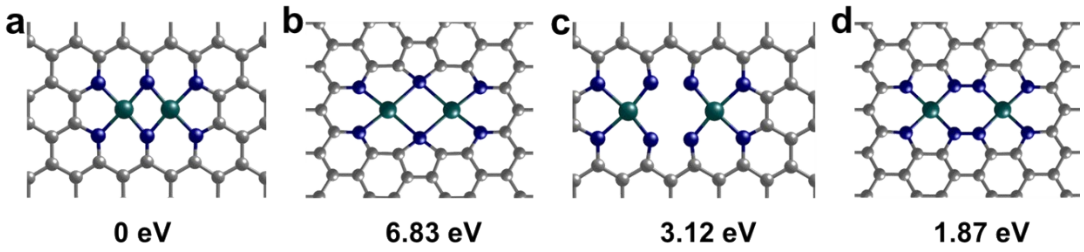

Fig. S13 According to the coordination structure of Fe_2N_6, we constructed four possible structural models. Through the stability comparison, it is found that the (a) model is the most stable, so we choose the first structure as the subsequent calculation model.

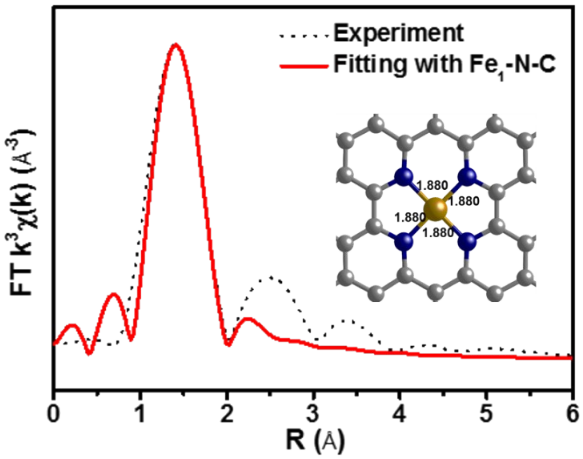

Fig. S14 The corresponding EXAFS fitting curves of Fe_1-N-C at *k* space and crystalline structures modeling of Fe_1-N-C for theoretical fitting analysis of EXAFS.

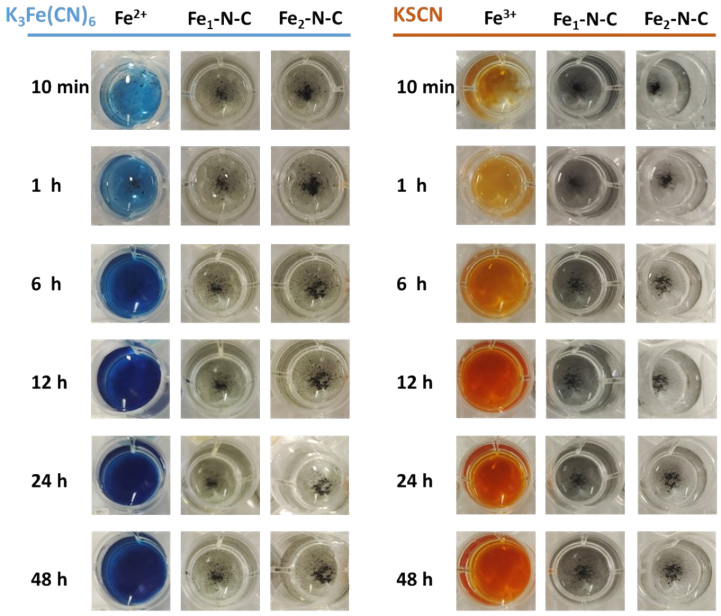

Fig. S15 The photos of potassium ferricyanide ($K_3Fe(CN)_6$) (a) and potassium thiocyanate (KSCN) (b) for monitoring the time-course ferrous and ferric ion releasing behaviors of Fe_x-N-C under pH 5.8 conditions.

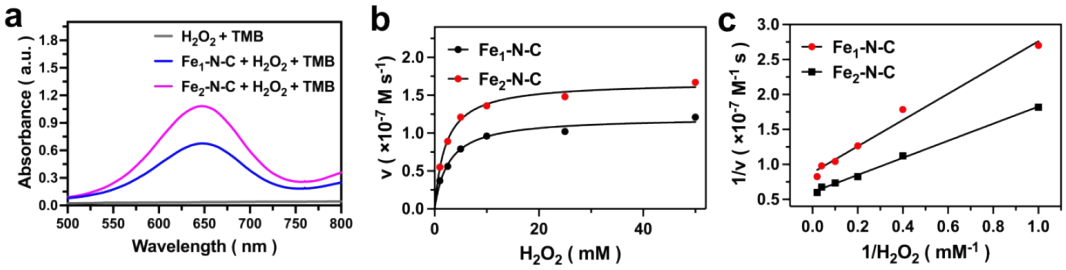

Fig. S16 (a) Absorbance spectra of TMB in different catalytic systems in the presence of H_2O_2. (b) Kinetic curves of Fe_x-N-C toward H_2O_2. (c) Lineweaver–Burk plot for Fe_x-N-C with H_2O_2 as a substrate.

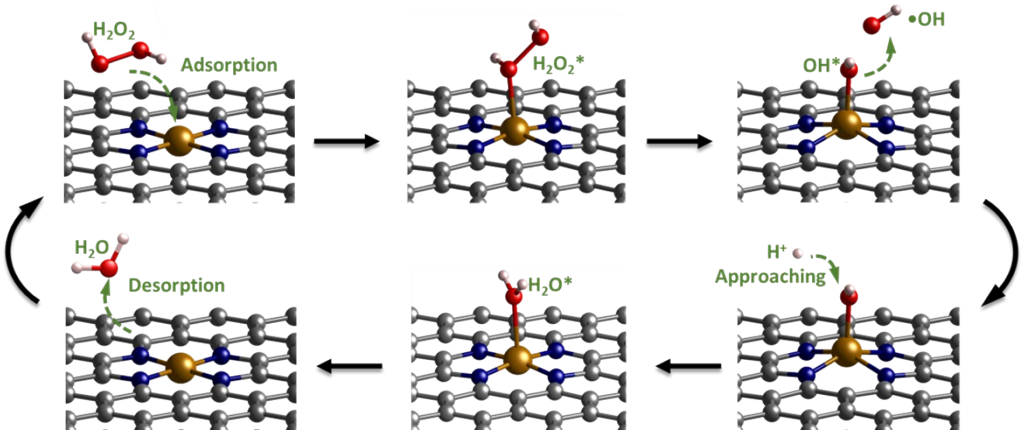

Fig. S17 The proposed catalytic mechanism for Fenton-like reaction of Fe_1-N-C.

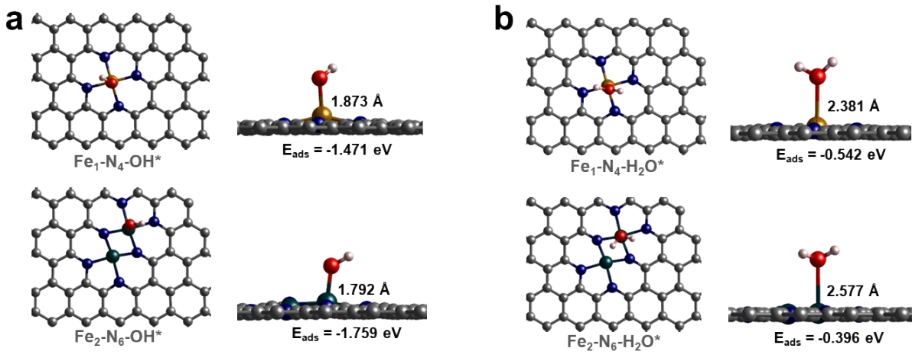

Fig. S18 OH* and H_2O* adsorption models in Fe_1-N-C and Fe_2-N-C.

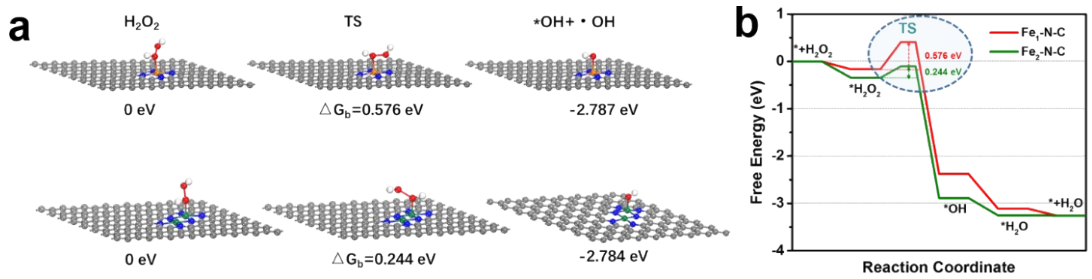

Fig. S19 Atomic structures of the initial state (left panel), transition state (middle panel), and final state (right panel) for: *H_2O_2 → *OH + •OH on the Fe site in Fe_1-N-C and Fe_2-N-C.

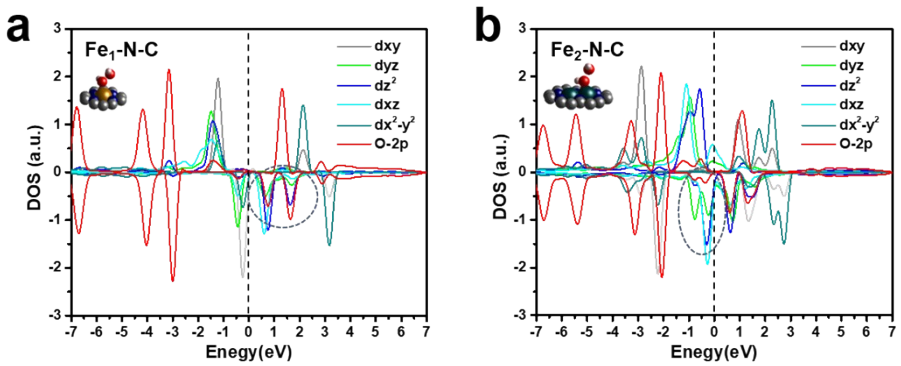

Fig. S20 (a-b) Computed projected density of states of Fe_1-N-C (a) and Fe_2-N-C (b) after H_2O_2* adsorption.

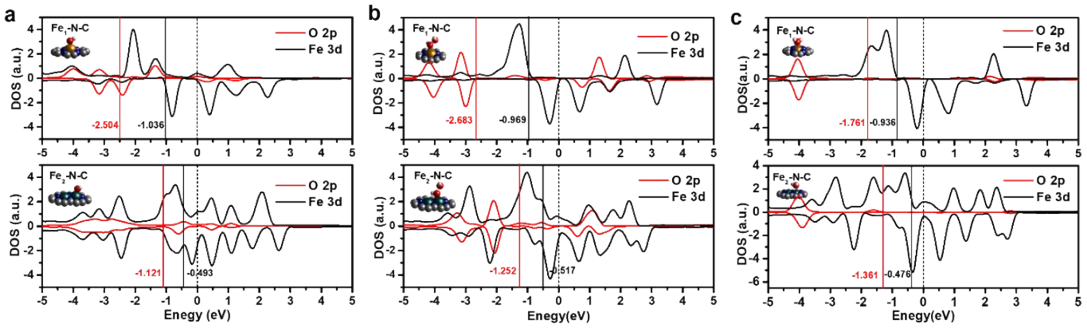

Fig. S21 The PDOS of OH* (a), H_2O_2* (b), and H_2O(c) adsorption state for Fe_1-N-C and Fe_2-N-C (The Fermi level is shown as the dash line. The *d*-band centers of Fe and the *p*-band centers of O are marked as solid lines for each sample).

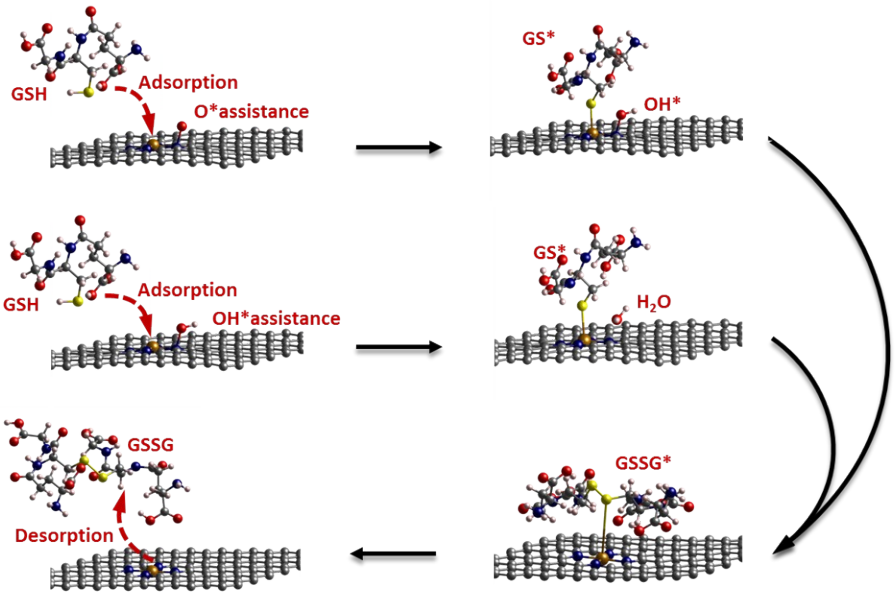

Fig. S22 The proposed catalytic mechanism for GSH consumption of Fe_1-N-C.

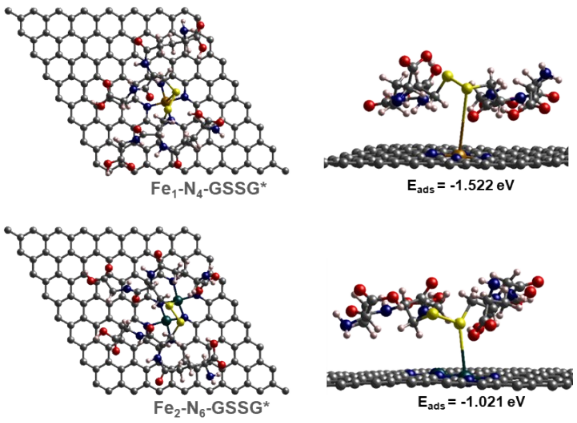

Fig. S23 GSSG* adsorption models in Fe_1-N-C and Fe_2-N-C.

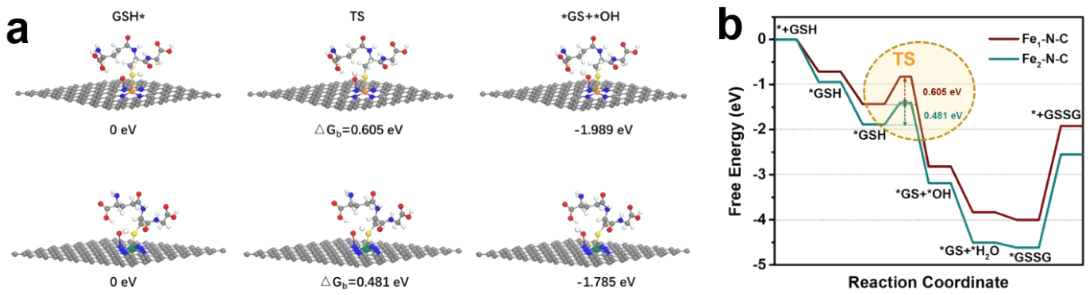

Fig. S24 Atomic structures of the initial state (left panel), transition state (middle panel), and final state (right panel) for: *GSH + O* → *GS + *OH on the Fe site in Fe_1-N-C and Fe_2-N-C.

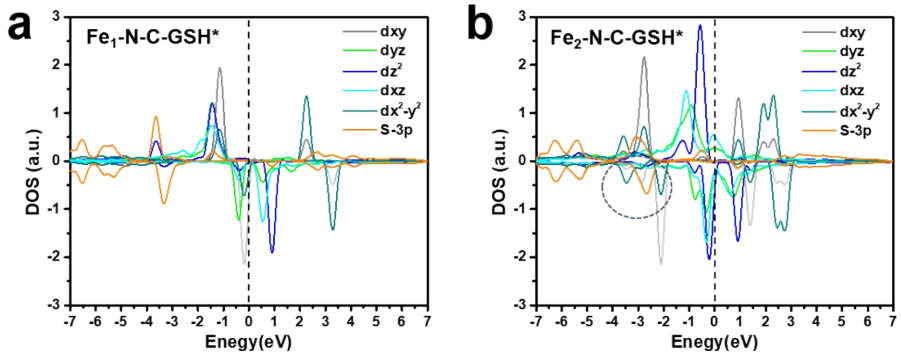

Fig. S25 (a-b) Computed projected density of states of Fe_1-N-C (a) and Fe_2-N-C (b) after GSH* adsorption.

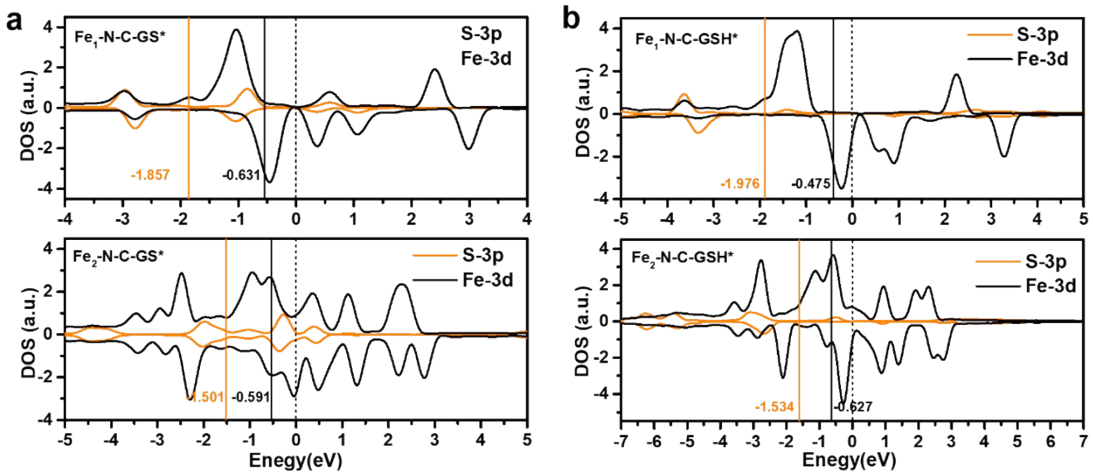

Fig. S26 The PDOS of GS* (a) and GSH* (b) adsorption state for Fe_1-N-C and Fe_2-N-C. The Fermi level is shown as the dash line. The *d*-band centers of Fe and the *p*-band centers of S are marked as solid lines for each sample.

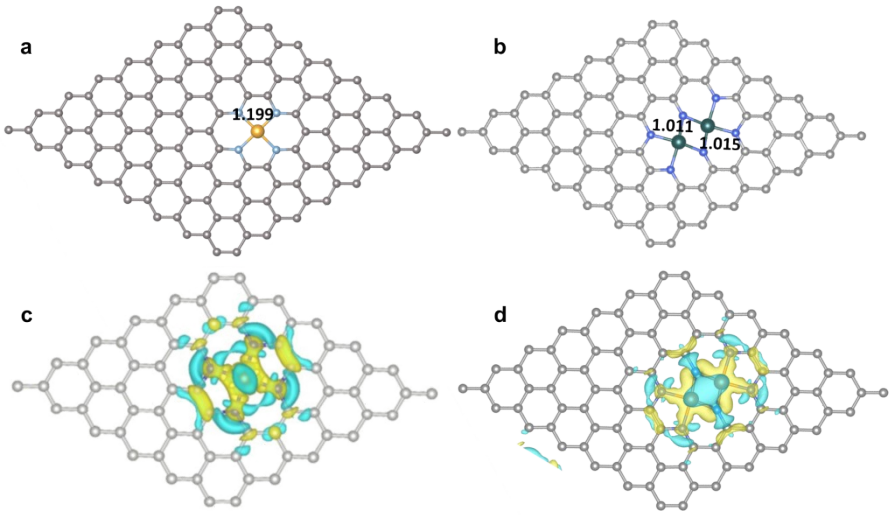

Fig. S27 Computed atomic net charge on Fe site in Fe_1-N-C (a) and Fe_2-N-C (b). Computed charge density differences for Fe_1-N-C (c) and Fe_2-N-C (d). Cyan and yellow areas represent charge density increase and decrease, respectively.

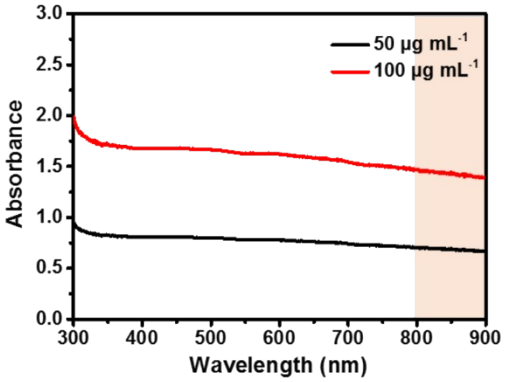

Fig. S28 UV-vis spectra of Fe_2-N-C dispersed in PBS at different concentrations.

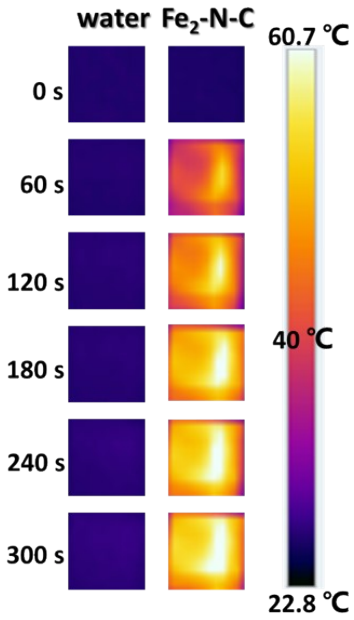

Fig. S29 Temperature change of Fe_2-N-C aqueous solution (200 μg mL^{-1}) irradiated with an 808 nm laser (1 W cm^{-2}) within 5 min.

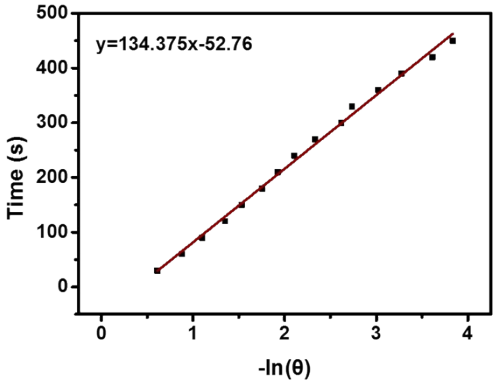

Fig. S30 Linear fit of time/-ln(θ) obtained during the cooling process.

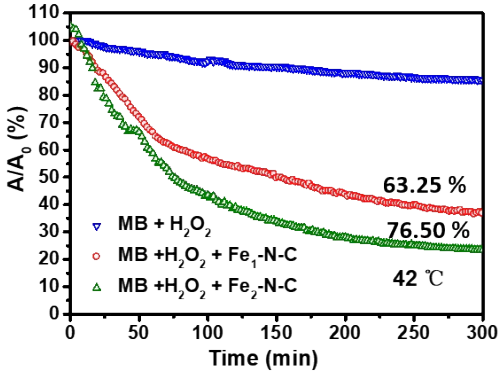

Fig. S31 Normalized absorbance of MB (A/A_0) upon the addition of Fe_x-N-C and H_2O_2 buffered in acidic PBS (pH = 5.8) under 42 ℃.

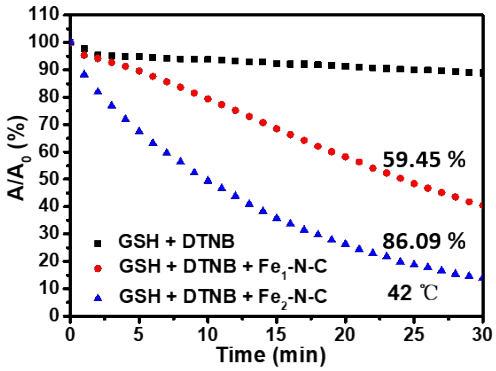

Fig. S32 Normalized absorbance of TNB (A/A_0) upon the addition of Fe_x-N-C and GSH buffered in acidic PBS (pH = 5.8) under 42 ℃.

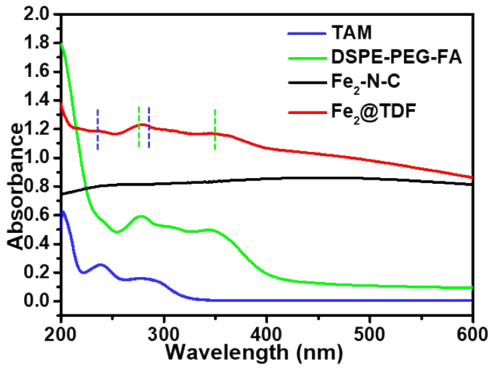

Fig. S33 UV-Vis spectra of TAM, DSPE-PEG-FA, Fe_2-N-C and Fe_2@TDF NEs.

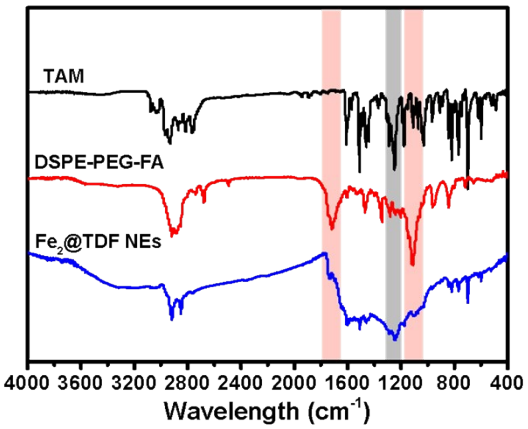

Fig. S34 FT-IR spectra of TAM, DSPE-PEG-FA, and Fe_2@TDF NEs.

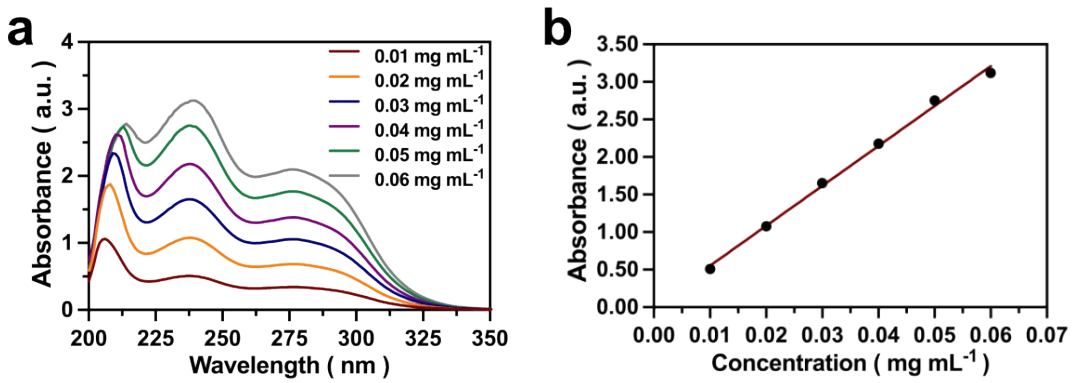

Fig. S35 (a) The UV-vis absorption spectra the different concentrations of free TAM and (b) the relevant standard curve at 238 nm.

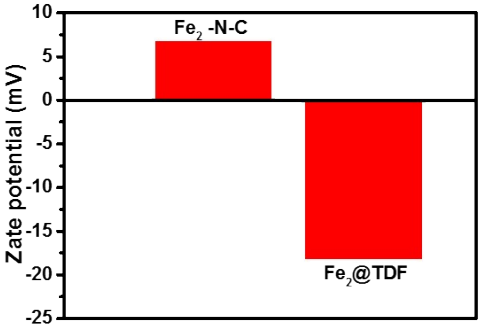

Fig. S36 The Zeta potential of Fe_2-N-C and Fe_2@TDF NEs in aqueous solution.

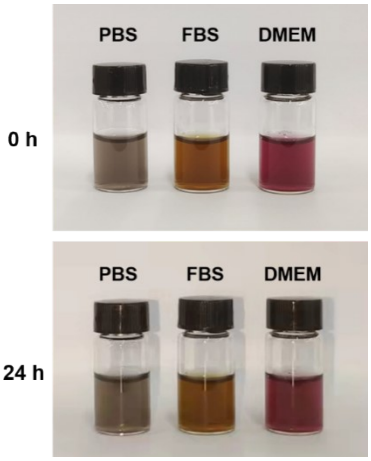

Fig. S37 Stability characterization of the Fe_2@TDF NEs dispersed in PBS, FBS, and DMEM medium, respectively.

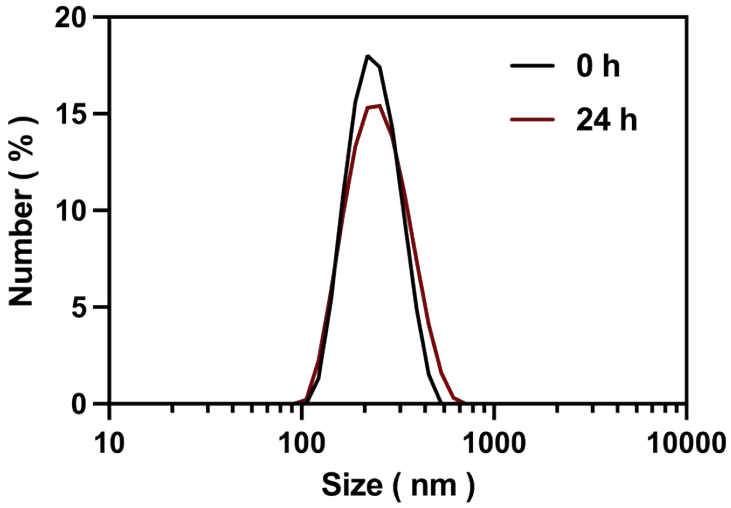

Fig.S38 Dynamic light scattering (DLS) of as-prepared Fe_2@TDF NEs stand for 0 h and 24 h.

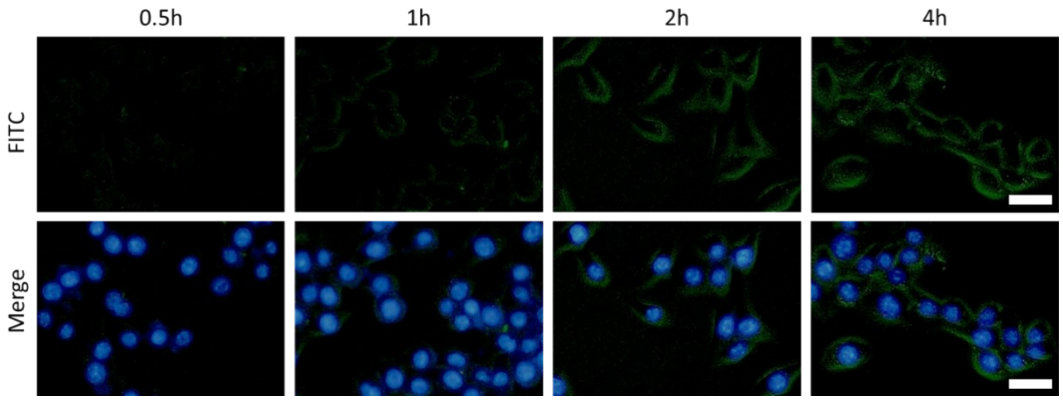

Fig. S39 Fluorescence images of 4T1 cells co-incubated with FITC labeled Fe_2@TDF NEs. (scale bars: 20 μm)

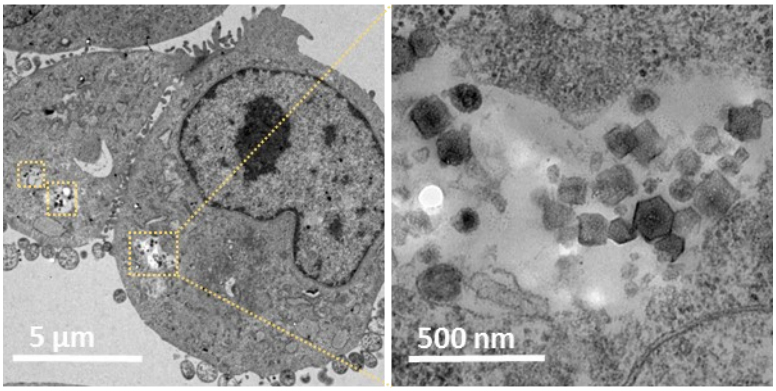

Fig. S40 The Bio-TEM images of 4T1 cells treated with Fe_2@TDF NEs.

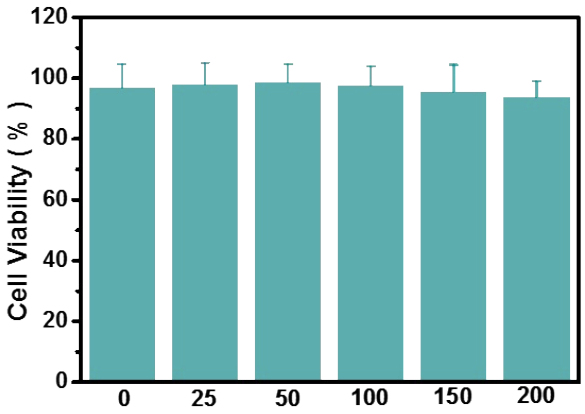

Fig. S41 Cytotoxicity assessment on LO2 cells with various coentrations of Fe_2@TDF NEs.

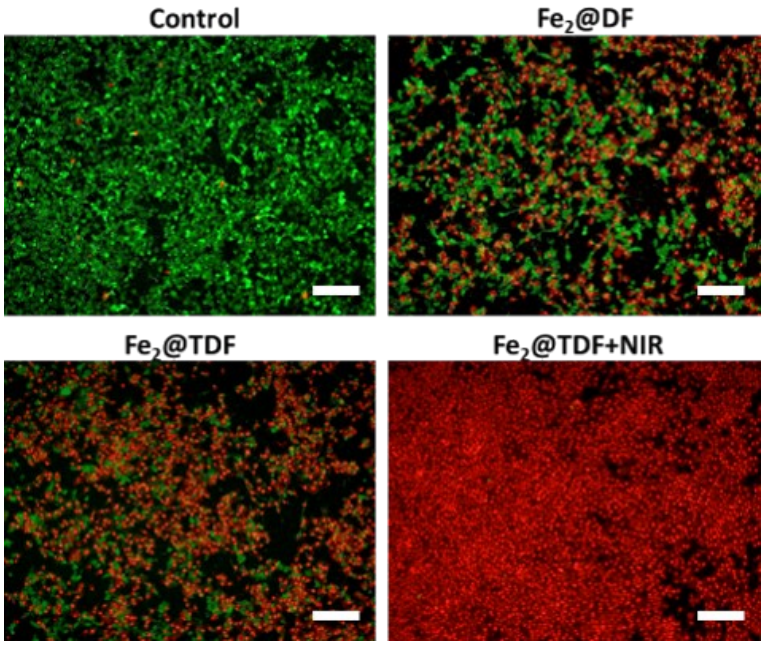

Fig. S42 Fluorescence images of Calcein AM (green, live cells) and PI (red, dead cells) after incubation with different materials for 24 h (Scale bars: 200 μm).

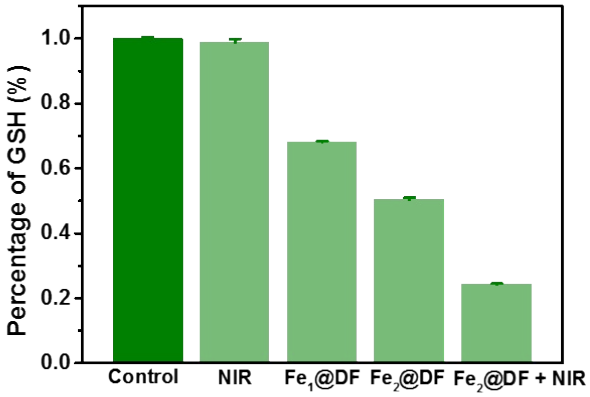

Fig. S43 Intracellular GSH detections of 4T1 cells with different treatments.

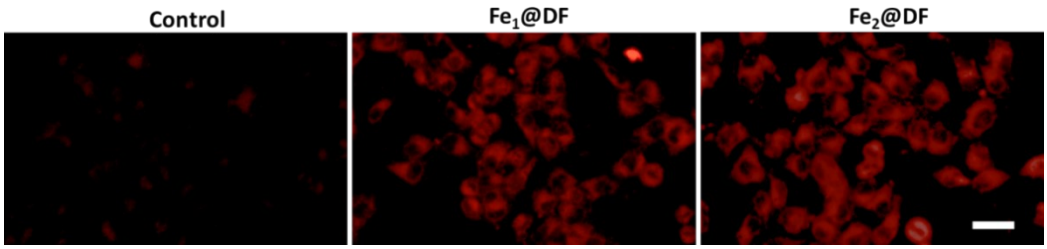

Fig. S44 The fluorescent images of C11-BODIPY labeled 4T1 cells after incubation with various materials (scale bars: 20 μm).

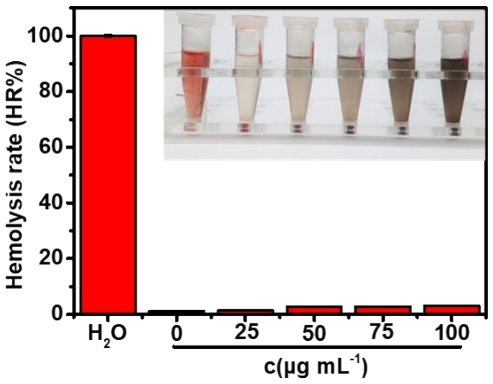

Fig. S45 Hemolysis rates of the RBC suspensions after treatment with various concentration of Fe_2@TDF (Inset: corresponding photograph of RBC samples).

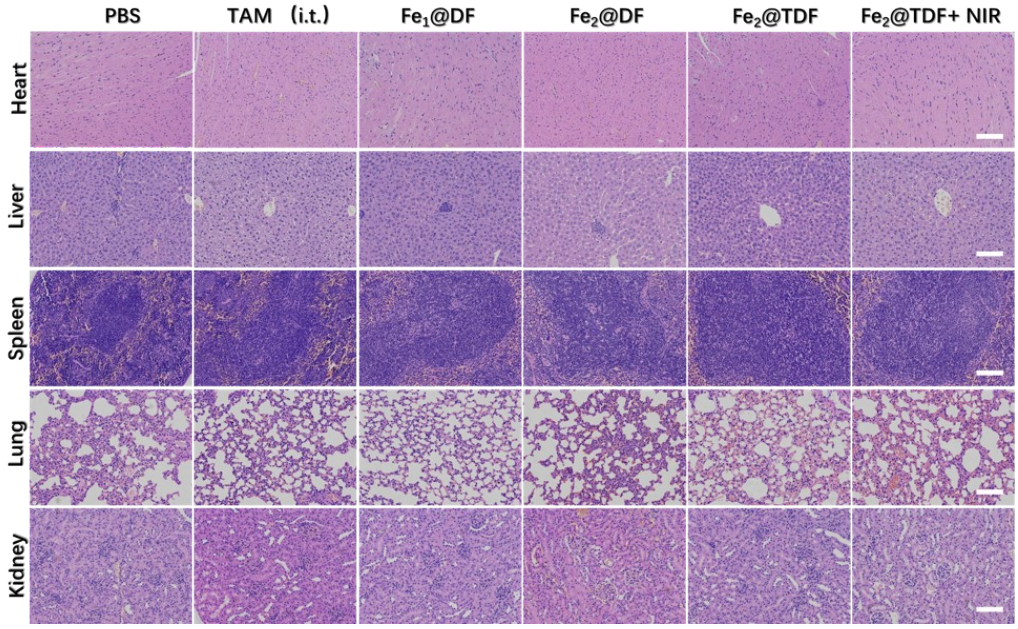

Fig. S46 Histological analysis of the major healthy organ via H&E staining after various treatments (Scale bars: 100 μm).

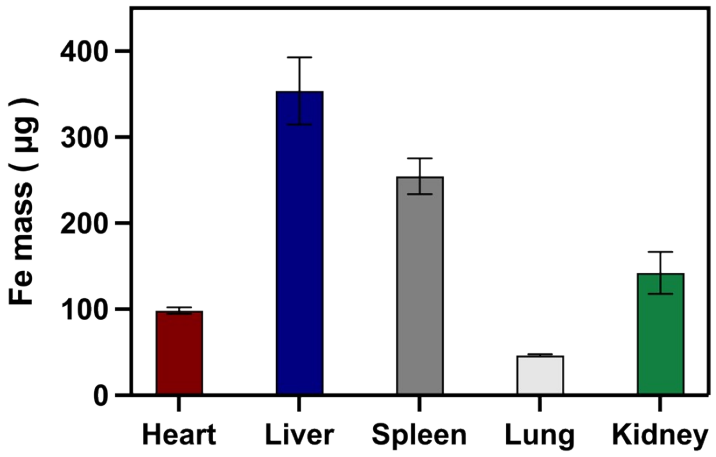

Fig. S47 The biodistribution of Fe in the major organs.

Table S1 Fitting parameters of Fe k-edge EXAFS curve fitting for Fe-foil, Fe_1-N-C and Fe_2-N-C samples.

Sample	Path	C.N.	R (Å)	$\sigma^2\times10^3$ (Å^2)	ΔE (eV)	R factor
Fe foil	Fe-Fe	8*	2.47±0.01	5.2±0.6	6.7±1.0	0.001
	Fe-Fe	6*	2.84±0.01	6.4±1.2	5.0±2.0	
Fe1-N-C	Fe-N/O	4.6	1.97±0.02	2.5±6.3	1.0±4.8	0.012
Fe2-N-C	Fe-N/O	5.2	1.98±0.03	12.0±0.1	1.4±3.9	0.0098
	Fe-Fe	1.2	2.51±0.02	4.9±2.7	-2.0±4.2	

Table S2 The mass percentages (%) of Fe and specific surface in Fe_1-N-C and Fe_2-N-C samples.

Sample	**Fe mass percentage (%)**
Fe_1-N-C	0.410
Fe_2-N-C	0.375

Table S3 The molar percentages (%) of pyridinic N, graphitic N and pyrrolic N in Fe_1-N-C and Fe_2-N-C samples.

Sample	Pyridinic N	Graphitic N	Pyrrolic N
Fe_1-N-C	29.18	65.20	5.62
Fe_2-N-C	31.88	62.47	5.65

Table S4 The Michaelis-Menton constant (K_m) and maximum reaction rate (V_{max}) of as prepared Fe_x-N-C and natural HRP with H_2O_2 as the substrate for POD-like catalysis.

Sample	Substrate	Km (mM)	Vmax (M s^{-1})	Reference
Fe_1-N-C	H_2O_2	2.664	1.208×10^{-7}	This work
Fe_2-N-C	H_2O_2	2.118	1.675×10^{-7}	This work
HRP	H_2O_2	3.71	8.71×10^{-8}	Nat. Nanotechnol., 2007, 2,577

4. Supplementary References

1. Kresse, G.; Furthmüller, J. Efficiency of Ab-Initio Total Energy Calculations for Metals and Semiconductors Using a Plane-Wave Basis Set. Comput. Mater. Sci. 1996, 6, 15-50.

2. Kresse, G.; Furthmüller, J. Efficient Iterative Schemes for Ab Initio Total-Energy Calculations Using a Plane-Wave Basis Set. Phys. Rev. B 1996, 54, 11169-11186.

3. Perdew, J. P.; Burke, K.; Ernzerhof, M. Generalized Gradient Approximation Made Simple. Phys. Rev. Lett. 1996, 77, 3865-3868.

4. Kresse, G.; Joubert, D. From Ultrasoft Pseudopotentials to the Projector Augmented-Wave Method. Phys. Rev. B 1999, 59, 1758-1775.

5. Blöchl, P. E. Projector Augmented-Wave Method. Phys. Rev. B 1994, 50, 17953-17979.